chemistry

MDPI

Article

Thermal Decomposition of Compounds Derived from 2H-Dihydropyran: A Computational Study

Pablo Ruiz [1,2,*], Sara Bucheli [1], Paula Fernández [1], Silvia Quijano [3], Jairo Quijano [1] and Jair Gaviria [1]

[1] Laboratory of Organic Physical Chemistry, School of Sciences, Universidad Nacional de Colombia, Medellin 050034, Colombia; sbucheli@unal.edu.co (S.B.); pfernandezc@unal.edu.co (P.F.); jquijano@unal.edu.co (J.Q.); jgarango@unal.edu.co (J.G.)
[2] School of Exact and Applied Sciences, Instituto Tecnológico Metropolitano, Medellin 050034, Colombia
[3] ECOBIO Group, Microbiology Program, School of Basic Sciences, Universidad Santiago de Cali, Santiago de Cali 763022, Colombia; silvia.quijano00@usc.edu.co
* Correspondence: paruizr@unal.edu.co

Abstract: This research study computationally examined the thermal decomposition of three molecules, 3,6-dihydro-2H-pyran, 4-methyl-3,6-dihydro-2H-pyran, and 2,6-dimethyl-3,6-dihydro-2H-pyran, using the PBE0/6-311+G(d,p) level of theory and a concerted mechanism with a 6-member cyclic transition state. For this analysis, kinetic and thermodynamic parameters were calculated for reactions within a temperature range of 584 to 633 K and compared with experimental data. Our results revealed that methyl substituents at 2, 4, and 6 positions decrease the activation free energy of the molecules. Even though the evaluated reactions exhibited high absolute synchronicity, significant differences were observed regarding the extent of their bond evolution.

Keywords: 4-methyl-3,6-dihydro-2H-pyran; 2,6-dimethyl-3,6-dihydro-2H-pyran; 3,6-dihydro-2H-pyran; functional PBE0; thermal decomposition

Citation: Ruiz, P.; Bucheli, S.; Fernández, P.; Quijano, S.; Quijano, J.; Gaviria, J. Thermal Decomposition of Compounds Derived from 2H-Dihydropyran: A Computational Study. *Chemistry* **2024**, *6*, 1385–1395. https://doi.org/10.3390/chemistry6060082

Academic Editor: Felix Plasser

Received: 29 September 2024
Revised: 29 October 2024
Accepted: 5 November 2024
Published: 7 November 2024

1. Introduction

Pyrans are six-membered heterocyclic molecules composed of five carbon atoms and one oxygen atom. They are non-aromatic with two double bonds and exist in two isomeric forms based on the position of the saturated carbon: 2-H-pyran and 4-H-pyran. Semi-saturated pyrans are labeled with the prefix "dihydro," while fully saturated variants are denoted as "tetrahydro" [1].

Pyrans are prevalent in numerous natural systems [2] and many of their derivatives exhibit notable biological properties [3–5], including antibacterial [6–8], antifungal [7,9], and herbicidal effects [2]. They are currently under extensive investigation for their potential use in targeted medical treatments [10], such as therapies for asthma and allergies [2], the development of antiepileptic drugs [11], and genetic disorders treatments [12]. Moreover, they have reported diuretic, anticoagulant [13], and anticancer properties [14]. Beyond medical applications, pyrans are also being explored for use in sensor and solar cell technologies [15,16]. 6-Benzoyl-3,4-dihydro-(2H)-pyran serves as a protecting group for triols in chemical synthesis [17,18].

Pyrans and their derivatives can be obtained from natural [19] compounds or synthesized and functionalized via chemical methods [7,14,20–22]. There is currently a growing trend toward using synthesis processes involving heterogeneous catalysts and environmentally friendly solvents [4,5,16,23,24].

The thermal decomposition of various dihydropyrans has been extensively studied and documented. In 1969, Wellington, C.A. [25] studied the thermolysis of 3,4-dihydro-2H-pyran, and in the same year, Caton, C.S. [26] examined the decomposition of 6-methyl-3,4-dihydro-2H-pyran. Frey et al. (1972) [27] reported findings on the decomposition of 2-methoxy-3,4-dihydro-2H-pyran, and in 1975, Collins et al. [28] conducted the thermal

decomposition of 2-methoxy-4-methyl-3,4-dihydro-2H-pyran in its cis and trans forms. In 1977, Bailey, I. and Frey, H. [29] investigated the decomposition of 2-ethoxy-3,4-dihydro-2H-pyran. In 1979, Frey, H. and Lodge, S. [30] reported the results of the thermal decomposition of 3,6-dihydro-2H-pyran. In another dihydropyran study in 1979, Frey et al. [31] examined the thermal decomposition of cis-2,6-dimethyl-3,6-dihydro-2H-pyran. In 1981, Frey, H. and Watts, H. [32] experimentally reported the thermolysis of 4-methyl-3,6-dihydro-2H-pyran. Other studies, such as those by Taylor (1988) [33] and Saito et al. (1990) [34], reported the results obtained from the decomposition reaction of 3,4-dihydro-2H-pyran. Saito followed this reaction using shock wave methodology at high temperatures [34]. The activation energy obtained was slightly higher than that reported in [33] but was similar to that obtained in [25].

Table 1 below lists the temperature range and activation energy of the experimental thermolysis obtained from the studies for each reaction.

Table 1. Thermal decomposition of Dihydro-2H-pyran compounds as reported in the literature [25–34].

Compound	Temperature Range (°C)	Ea (kJ·mol^{-1})
3,4-dihydro-2H-pyran	316–389	219.4
3,4-dihydro-2H-pyran	343–393	209.0
3,4-dihydro-2H-pyran	990–1245	215.9
6-methyl-3,4-dihydro-2H-pyran	330–370	214.2
2-methoxy-3,4-dihydro-2H-Pyran	296–353	203.1
2-methoxy-4-methyl-3,4-dihydro-2H-pyran	287–345	201.5 (trans) 196.0 (cis)
2-ethoxy-3,4-dihydro-2H-pyran	288–355	202.1
3,6-dihydro-2H-pyran (DHP)	329–374	208.1
cis-2,6-dimethyl-3,6-dihydro-2H-pyran (DMDHP)	300–351	196.3
4-methyl-3,6-dihydro-2H-pyran (MDHP)	311–361	209.5
2-methyl-3,4-dihydro-2H-pyran	364–393	191.5

The data presented in Table 1 demonstrate that investigated dihydro-2H-pyran compounds effectively reduce the activation energy of the reaction. This reduction is mainly attributed to the presence of substituent groups in the molecular structure, particularly when these groups are located at the 2 position. Discrepancies exist among the reported results for 3,4-dihydro-2H-pyran.

However, all of the cited studies agreed that the decomposition of the studied dihydropyran compounds occurs through homogeneous, first-order, unimolecular, and concerted reactions. The same conclusions were obtained for the thermal decomposition of 2-phenoxytetrahydro-2H-pyran [35]. The authors propose the presence of a highly asymmetric activated complex, specifically a transition state that exhibits slight polarity. In this state, the breaking of the O1-C6 bond is more advanced compared to the cleavage of the C2-C3 bond. As a result, a positive charge forms on C2 while a negative charge develops on the oxygen atom.

In this research, we applied computational tools using density functional theory (DFT) to study the reactions of 3,6-dihydro-2H-pyran, unsubstituted and substituted with a methyl group at position 4 and simultaneously at positions 2 and 6. The results were compared against reported experimental data, offering a deeper understanding of transition state structures, the impact of substituent groups, bond changes, and the synchronicity of the reaction.

2. Methods

This study examined the potential energy surface for the thermal decomposition of 3,6-dihydro-2H-pyran, 4-methyl-3,6-dihydro-2H-pyran, and 2,6-dimethyl-3,6-dihydro-2H-pyran using DFT. After optimizing the geometries, vibrational frequency calculations were performed using the functional PBE0 [36] and the 6-311+G(d,p) basis set [37], as implemented in Gaussian 09 [38]. Each structure in the decomposition reaction was

identified as either a minimum (for reactants and products) or a saddle point (for transition states). It was verified that the frequencies of the minimum points present only real values and the structures associated with the transition states were characterized by having one and only one imaginary frequency.

The transition state structures were then used in Intrinsic Reaction Coordinate calculations [39] to confirm their connection to the corresponding minimum values for the reactant and product (the results can be seen in Figures S1–S3 of the supporting information).

All DFT-optimized structures were subjected to stability analysis in the Gaussian 09 software [38].

These vibrational frequency calculations provided values for the zero-point energy (ZPE) and allowed for the determination of the kinetic and thermodynamic parameters for each reaction. ZPE values were scaled by a factor of 0.9812, following the recommendations of Merrick et al. (2007) [40].

The enthalpies and entropies of each molecule were calculated using standard thermodynamic equations [41]. Computational calculations were conducted at various temperatures (584, 600, 608, and 633 K) under a constant pressure of 1 atm.

Activation parameters and rate constants were determined using the classical framework of Transition State Theory (TST) based on the Eyring Polanyi equations [42,43].

The Natural Bond Orbital (NBO) technique [44,45], implemented via the NBO program [46] within the Gaussian 09 software package, was used to obtain the total natural atomic charges. These charges facilitate the calculation of Wiberg bond indices (β_i) [47,48], which are employed to monitor the progression of the studied reactions. The relative evolution of bond formation or breaking processes can be defined as

$$\delta\beta_i = \left(\beta_i^{TS} - \beta_i^{R}\right) / \left(\beta_i^{P} - \beta_i^{R}\right) \quad (1)$$

Then, the percentage of bond evolution (%EV) is evaluated using

$$\%EV = \delta\beta_i \times 100 \quad (2)$$

where ${\beta_i}^{TS}$, ${\beta_i}^{R}$, and ${\beta_i}^{P}$ represent the Wiberg bond indices for bond i in the transition state, reactant, and product structure, respectively. The degree of progress of the transition state in the reaction can be inferred from the average relative variation ($\delta\beta$av), considering the number of bonds (n) directly involved in the breaking and formation processes; then,

$$\delta\beta_{av} = \sum_i^n \delta\beta_i / n \quad (3)$$

This reaction is characterized by absolute synchronicity (Sy), calculated from the Wiberg bond indices. Furthermore, the reaction is determined as follows:

$$S_y = 1 - \left[1/(2n-2)\sum|\delta\beta_i - \delta\beta_{av}|/\delta\beta_{av}\right] \quad 0 \le S_y \le 1 \quad (4)$$

where a value close to one indicates as a highly synchronous reaction.

3. Results and Discussion

3.1. Reaction Mechanism

The thermal decomposition of 3,6-dihydro-2H-pyran (DHP), 4-methyl-3,6-dihydro-2H-pyran (MDHP), and 2,6-dimethyl-3,6-dihydro-2H-pyran (DMDHP) was studied computationally using the reaction mechanism depicted in Figure 1. In this mechanism, electron movement within the ring triggers simultaneous bond formation and breaking, resulting in a concerted six-membered transition state. During product formation, the decomposition of DHP and MDHP generates formaldehyde, along with 1,3-butadiene and 2-methyl-1,3-butadiene, respectively. The decomposition of DMDHP produces acetaldehyde and 1,3-pentadiene.

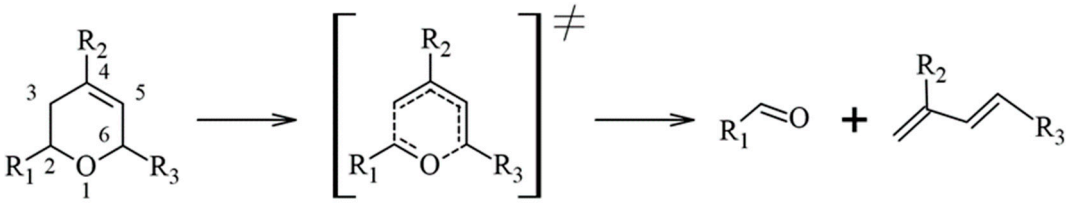

Figure 1. Mechanism of the thermal decomposition of 3,6-dihydro-2H pyran compounds. DHP: R1 = R2 = R3 = H; MDHP: R1 = R3 = H, R2 = Me; DMDHP: R1= R3 = Me; R2 = H.

3.2. Structure Optimization

Preliminary optimization and frequency calculations for the thermal decomposition of DHP, MDHP, and DMDHP were conducted using the functionals B3LYP, M06-2X, PBE0, and ωB97xD and the Post-Hartree-Fock method (MP2), in the temperature range of 584–633 K. Among these, the functional PBE0 in conjunction with the 6-311+G(d,p) basis set yielded the activation energy (Ea) closest to the experimental value reported in the literature. The ωB97xD and M06-2X functionals overestimated Ea, whereas the B3LYP functional and MP2 method produced a lower value, although the results of the latter are also close to the experimental value (see Table 2). Therefore, the structures involved in the mechanisms of the three reactions were optimized at the PBE0/6-311+G(d,p) level. Figure 2, below, denoted the optimized structures of the reactants and transition states for each reaction studied. The obtained imaginary frequencies were 515, 482, and 503 cm^{-1} for DHP, MDHP, and DMDHP, respectively. The distances of bonds involved in the reaction center are shown in Table S5 of the Supplementary Material.

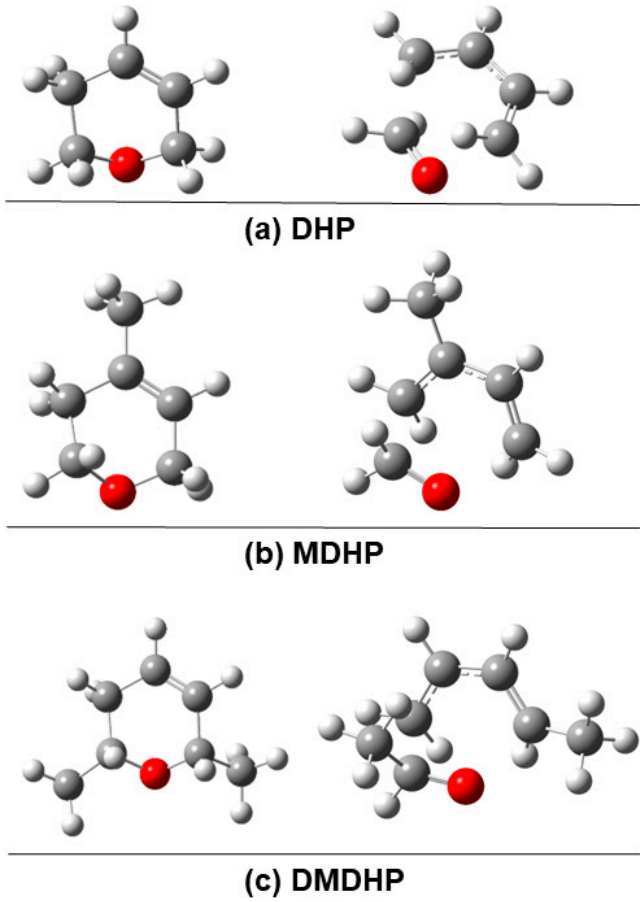

Figure 2. Molecules optimized at the PBE0/6-311+G(d,p) level for the reactants and transition states of the decomposition of DHP, MDHP, and DMDHP according to the reaction mechanism depicted in Figure 1.

Table 2. Activation energies (Ea) of the decomposition of DHP, MDHP, and DMDHP with different computational methods. The deviation from the experimental value is shown in parentheses. Experimental values were taken from [32].

	Ea (kJ·mol^{-1})					
	Computational Method					Experimental
Reaction	B3LYP	M062X	PBE0	ωB97XD	MP2	
DHP	185.4 (10.9%)	221.2 (6.3%)	214.3 (2.9%)	217.5 (4.6%)	199.6 (4.0%))	208
MDHP	186.1 (11.4%)	221.7 (5.6%)	215.0 (2.4%)	217.1 (3.4%)	200.3 (4.6%)	210
DMDHP	175.3 (10.6%)	210.5 (7.4%)	202.1 (3.1%)	206.6 (5.4%)	193.3 (1.4%)	196

3.3. Reaction Kinetics

Computational modeling at the PBE0/6-311+G(d,p) level for the thermal decomposition reactions of the studied molecules allowed the determination of the activation parameters, which are presented in Table 3. The first-order rate constants at each temperature were calculated by TST. The linearization of the Arrhenius equation (shown in Figure 3) provides the activation energy (Ea) and frequency factor (A) of each reaction. Experimental values were taken from [32].

Table 3. Activation Free Energy ($\Delta G^{\neq}$), Enthalpy ($\Delta H^{\neq}$), and Entropy ($\Delta S^{\neq}$); Activation Energy (Ea) and Frequency Factor (A) for Thermolysis of Compounds derived from 2H-pyran. Calculated at the PBE0/6-311+G(d,p) Level at 600 K. Experimental parameters are shown in parentheses.

Compound	$\Delta G^{\neq}$ (kJ·mol^{-1})	$\Delta H^{\neq}$ (kJ·mol^{-1})	$\Delta S^{\neq}$ (J-mol^{-1}·K^{-1})	Ea (kJ·mol^{-1})	Log A (s^{-1})
DHP	196	208	20	214 (208)	14.59 (14.31)
MDHP	190	209	33	215 (210)	15.24 (14.62)
DMDHP	183	196	21	202 (196)	14.66 (19.91)

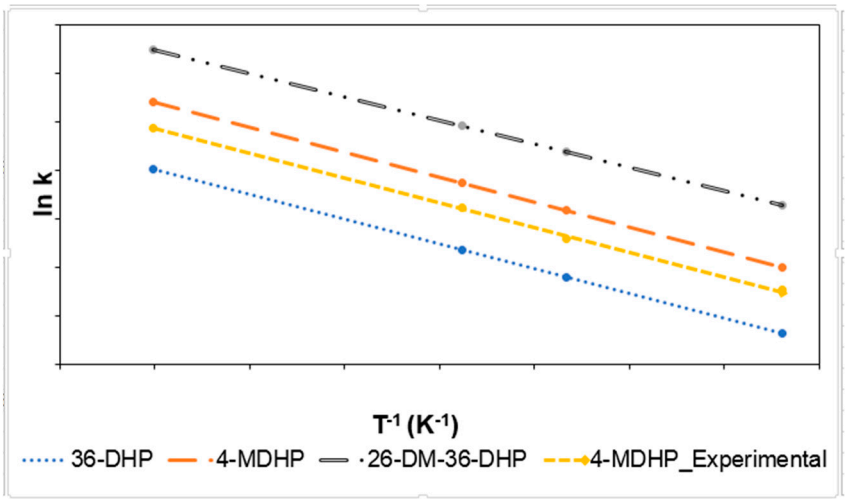

Figure 3. Linearization of the Arrhenius equation for the thermal decomposition of 2-H-pyran Derivatives. Based on the computational data.

From the obtained computational results, the lowest values for $\Delta G^{\neq}$ and Ea (183 and 202 kJ·mol^{-1}, respectively) occurred in the decomposition of DMDHP. It is evident that

the substituent groups used on the base structure of 3,6-dihydro-2H-pyran favor thermal decomposition by at least 6 kJ·mol^{-1} in the activation free energy value per methyl group. Specifically, the values are 196, 190, and 183 kJ·mol^{-1} for DHP, MDHP, and DMDHP, respectively.

In addition to the molecules presented in Table 3, calculations were also performed for the DHP structure with a single substituent at positions 2 and 6 (2-methyl-3,6-dihydro-2H-pyran and 6-methyl-3,6-dihydro-2H-pyran). For 2-methyl-3,6-dihydro-2H-pyran, $\Delta G^{\neq}$ was 182 kJ·mol^{-1} and Ea was 202 kJ·mol^{-1}, while for 6-methyl-3,6-dihydro-2H-pyran, the values were 184 and 204 kJ·mol^{-1}, respectively. The results indicate that the key positions for the thermal decomposition of DHP compounds are 2, 6, and 4, in that order.

Contrasting the above with the results in the kinetic parameters of the decomposition of DMDHP whose molecule is simultaneously substituted in positions 2 and 6, it can be observed in the values of $\Delta G^{\neq}$ and Ea that there is no additive effect of both substituent groups in promoting the reaction; basically, the stabilizing effect on the activated complex for the decomposition of DMDHP can be attributed to the methyl group in position 2, confirming that this is the key position that favors the thermal decomposition of 3,6-dihydro-2H-pyrans.

The calculated NBO atomic charges for the studied reactions show that the greatest decrease in electronic density from the reactant to the transition state occurs at C2 and C4 atoms. Table 4 presents the NBO charges for atoms Ci, where i = 2,4 in the reactant q^{R}Ci and in the transition state q_{TS}Ci. For example, in the thermolysis of DHP, the C2 atom of the reactant has a charge of −0.036, but in the transition state, this charge becomes 0.103, a change of 0.139. (Please refer to the Supplementary Material for complete data).

Table 4. Natural Atomic Charges for Reactants (q^{R}) and transition states (q^{TS}) at C2 and C4 atoms for the thermal decomposition reaction of DHP, MDHP, and DMDHP. Calculated at the PBE0/6-311+G(d,p) level.

Reaction	DHP	MDHP	DMDHP
q^{R}_{C2}	−0.036	−0.034	0.121
q^{TS}_{C2}	0.103	0.103	0.260
q^{R}_{C4}	−0.196	−0.017	−0.186
q^{TS}_{C4}	−0.132	0.050	−0.126

The obtained activation energies (Ea) agree well with the experimental values, with the computational results showing an approximate overestimation of 6 kJ·mol^{-1}. The MDHP reaction exhibits the highest barrier, but its activation-free energy ($\Delta G^{\neq}$) is not the highest among the reactions studied. Instead, $\Delta S^{\neq}$ is the highest for MDHP, indicating that its transition state has greater freedom and is thus subject to more significant molecular interactions.

This result is further supported by the highest $\Delta H^{\neq}$ value observed for MDHP compared to the other reactions. For instance, in the transition state of MDHP, the O1-C6 bond distance measures 2.21 Å, while the corresponding distances for DHP and DMDHP are 2.17 and 2.16 Å, respectively. A comparison of the kinetic parameters reveals that the methyl group at position 4 in MDHP enhances the reaction by its entropic contribution.

For the decomposition of DHP, MDHP, and DMDHP, the rate constants at 600 K were obtained as 1.02×10^{-4}, 3.99×10^{-4}, and 1.36×10^{-4} s^{-1}, respectively. Regarding DHP, the relative rate constants are 3.9 and 13.3 for MDHP and DMDHP, respectively. Experimentally [32], the reported relative constants are 1.6 and 4.3. Although the calculated values differ from the theoretical values, the relative order of the reaction rates remains consistent.

Figure 3 depicts the linearization of the Arrhenius equation using data from the computational study and experimental MDHP kinetics. This figure highlights how the substituent effect on the ring enhances the first-order rate constant at each temperature. The Arrhenius line for the experimental decomposition of MDHP closely aligns with the computationally obtained values.

The energy profile of the studied reactions is illustrated in Figure 4. This figure compares the progress of the thermolysis reactions of DHP, MDHP, and DMDHP. The decomposition of DMDHP is characterized by having the lowest value for $\Delta G^{\neq}$ and also producing more stable products, with $\Delta G_{600} = -33.8$ kJ·mol^{-1}. The MDHP thermolysis has a lower $\Delta G^{\neq}$ compared to DHP, as shown in Table 2 and Figure 4. However, the products generated from MDHP have higher free energy ($\Delta G_{600} = 8.5$ kJ·mol^{-1}) compared to 5.2 kJ·mol^{-1} for the DHP reaction.

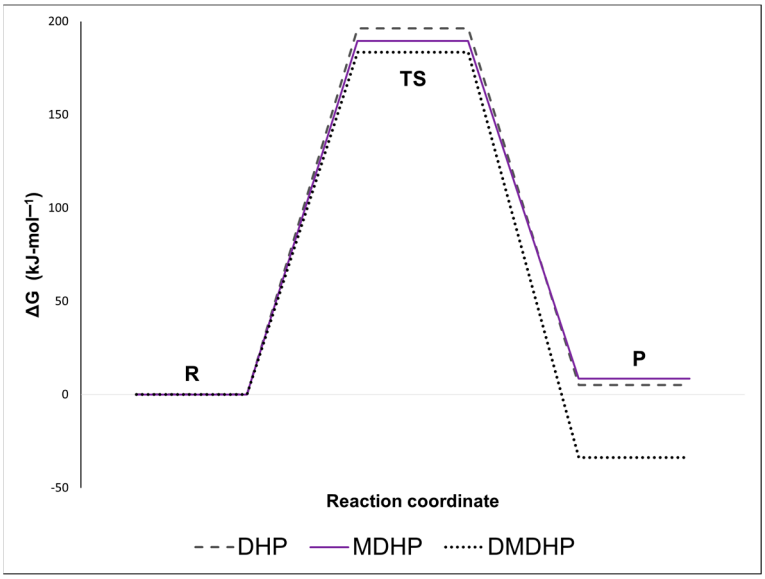

Figure 4. Energy profile of the thermal decomposition of DHP, MDHP, and DMDHP.

3.4. Population Analysis (NBO)

The calculation of NBOs for the DHP, MDHP, and DMDHP molecules allowed the determination of Wiberg bond indices, which are listed in Table 5.

Table 5. Wiberg Bond Indices of Reactants, transition states, and products, β_i^R, β_i^{TS}, β_i^P. Percentage of evolution (%EV), average bond evolution degree in the transition state (δβav), and absolute synchronicity (Sy) for the thermolysis of DHP (first entry), MDHP (second entry), and DMDHP (third entry). Calculated at the PBE0/6-311+G(d,p) level. (See Figure 1 for atom labeling).

	O1-C2	C2-C3	C3-C4	C4-C5	C5-C6	C6-O1
β_i^R	0.918	1.013	1.034	1.910	1.034	0.930
	0.921	1.012	1.015	1.846	1.033	0.929
	0.894	0.998	1.034	1.917	1.012	0.906
β_i^{TS}	1.449	0.483	1.433	1.363	1.574	0.266
	1.448	0.496	1.394	1.309	1.605	0.242
	1.399	0.490	1.409	1.393	1.493	0.266
β_i^P	1.944	0	1.890	1.128	1.890	0
	1.944	0	1.831	1.097	1.893	0
	1.879	0	1.885	1.131	1.827	0
%EV	51.7	52.3	46.7	69.9	63.1	71.4
	51.5	51.0	46.4	71.7	66.5	74.0
	51.3	50.9	44.1	66.6	59.1	70.6
δβav	0.59		Sy	0.93		
	0.60			0.92		
	0.57			0.94		

The percentages of evolution offer insights into the progression of bond-breaking and formation processes. Table 5 reveals that the bonds on the right side of the molecules—specifically, the C4-C5, C5-C6, and C6-O1 bonds—exhibit the highest evolution values. This

suggests that this region of the molecule is more reactive, largely due to the presence of the double bond and oxygen atom. The most advanced procedure is the breaking of the C6-O1 bond. For instance, the degree of evolution for MDHP is 74%, which corresponds to the longest bond length observed. In addition, the breaking of the C4-C5 double bond in the pyran ring shows nearly 72% advancement of MDHP.

Based on the %EV values, it can be inferred that the electronic redistribution in the reaction starts with the breaking of the C6-O1 bond. The electrons stay on the oxygen atom rather than immediately shifting to form the O1-C2 bond, resulting in an electron-deficient C6 atom. This condition favors the presence of a methyl group as a substituent at position 6. Above the ring, the C4-C5 double bond breaks, causing electrons to flow toward the formation of the C5-C6 double bond. This results in the electron deficiency of the C4 atom, making the decomposition process more favorable when a methyl group is present at this position. Similarly, the breaking of the C2-C3 bond renders the C2 atom electron-deficient, which is also favored by the presence of a methyl group. Subsequently, the O1-C2 bond forms and the process concludes with the formation of a double bond between the C3 and C4 atoms.

Bond deficiency in the transition state, determined by summing the percentages of broken bonds and subtracting the sum of formed bonds, yields positive values of 10.7%, 10.8%, and 11.2% for DHP, MDHP, and DMDHP, respectively. This analysis suggests that electrons involved in the broken bonds of the activated complexes do not immediately undergo new bond formation. Instead, they remain on certain atoms, inducing polarity within the molecular structure.

When substituents were added at positions 2 and 6, bond-breaking and bond-formation processes were slowed relative to the unsubstituted molecule. Specifically, the average bond evolution degree ($\delta\beta$av) was 0.57, compared to values of 0.59 and 0.60 in the decomposition of DHP and MDHP, respectively. Consequently, the activation enthalpy for the decomposition of DMDHP was also the lowest. Overall, the $\delta\beta$av values indicate that the transition states were advanced, meaning that they more closely resemble the product molecules than the reactants.

The calculated absolute synchronicity values were 0.93, 0.92, and 0.94 for the DHP, MDHP, and DMDHP reactions, respectively, which are considered synchronous reactions with values above 0.9. The experimental thermal decomposition of comparable molecules was conducted and classified these processes as asynchronous, concentrated on the evolution of two specific bonds. In contrast, the quantitative approach used here accounts for all bonds involved in the transformation processes during the chemical reaction.

Our computational results show that the polarities of the transition state structures in the decomposition reactions of DHP, MDHP, and DMDHP are 2.0209, 2.9355, and 1.5443 Debyes, respectively. These values maintain a certain proportionality with the calculated synchronicity values for each reaction.

4. Conclusions

The addition of methyl substituent groups on 3,6-dihydro-2H-pyran compounds favors their thermal decomposition; the stabilizing effect is given by the decrease in the electron density of some of the carbon atoms in the pyran ring of the transition state. The parameters obtained in the reactions studied also allow us to think that position 2 of the ring is key in the stabilization process of the activated complex.

The kinetic parameters of the reactions studied indicate that there is no additive effect of simultaneous substituent groups in promoting the reaction.

Although the energy barrier for MDHP breakdown is larger than that observed for DHP, the activation-free energy is lower due to the entropic effect.

The transition states in the reactions studied show a more reactive molecular region that includes a double bond and the oxygen atom.

Although the reactions can be considered concerted and exhibit high absolute synchronicity, relative asynchronous effects are observed in the O1-C6 and C2-C3 bonds, leading to a notable charge disparity on the O1 and C2 atoms.

Supplementary Materials: The following supporting information can be downloaded at https://www.mdpi.com/article/10.3390/chemistry6060082/s1: Table S1: PBE0/6-311+G(d,p)-optimized cartesian coordinates for all the species involved in the thermal decomposition of 3,6-dihydro-2H-pyran (DHP), in gas phase; Table S2: PBE0/6-311+G(d,p)-optimized cartesian coordinates for all the species involved in the decomposition of 4-methyl-3,6-dihydro-2H-pyran (MDHP), in gas phase; Table S3: PBE0/6-311+G(d,p)-optimized cartesian coordinates for all the species involved in the decomposition of 2,6-dimethyl-3,6-dihydro-2H-pyran (DMDHP), in gas phase; Table S4: NBO charges for reactants (q^R) and transition states (q^{TS}) in the reaction coordinate for thermal decomposition of 3,6-dihydro-2H-pyran, 4-methyl-3,6-dihydro-2H-pyran and 2,6-dimethyl-3,6-dihydro-2H-pyran. Calculated at PBE0/6-311+G(d,p); Table S5: Bond distances (Å) of the atoms of the transition state involved in each decomposition reaction; Figures S1–S3: Intrinsic Reaction Coordinate for thermal decomposition of DHP, MDHP, and DMDHP. Calculated at PBE0/6-311+G(d,p).

Author Contributions: The contribution of each author listed is based on conceptualization, P.R.; methodology, S.B. and P.F.; formal analysis, P.R., J.G. and J.Q.; investigation, P.R. and S.Q.; writing—original draft preparation, P.R.; writing—review and editing, S.Q., J.G. and J.Q. All authors have read and agreed to the published version of the manuscript.

Funding: This research has been funded by Dirección General de Investigaciones of Universidad Santiago de Cali under call No. 01-2024.

Data Availability Statement: The original contributions presented in the study are included in the article/Supplementary Material; further inquiries can be directed to the corresponding author.

Acknowledgments: The authors would like to express their gratitude to the Universidad Nacional de Colombia—Medellín Campus for the support received during the research stage. "This research has been funded by Dirección General de Investigaciones of Universidad Santiago de Cali under call No. 01-2024". P.R would also like to thank the Instituto Tecnológico Metropolitano (ITM), Medellín—Colombia.

Conflicts of Interest: The authors declare no conflicts of interest.

References

1. Mcnaught, A.D.; Smith, P.A.S.; García Alcolea, E. *Nomenclatura de Compuestos Heterociclos*; Ediciones de la Universidad de Murcia (Editum): Murcia, Spain, 1992; pp. 91–122.
2. Abrishami, F.; Teimuri-Mofrad, R.; Bayat, Y.; Shahrisa, A. Synthesis of some aldoxime derivatives of 4H-pyran-4-ones. *Molecules* **2002**, *7*, 154–196. [CrossRef]
3. Eskandari, K.; Rafieian-Kopaei, M. Synthesis of 5,6-dihydro-2H-pyran-2-ones (microreview). *Chem. Heterocycl. Compd.* **2016**, *52*, 158–160. [CrossRef]
4. Kate, P.; Pandit, V.; Jawale, V.; Bachute, M.L. Proline catalyzed one-pot three-component synthesis and evaluation for biological activities of tetrahydrobenzo[b]pyran: Evaluation by green chemistry metrics. *J. Chem. Sci.* **2022**, *134*, 4. [CrossRef]
5. Borah, B.; Dwivedi, K.D.; Chowhan, L.R. Review on synthesis and medicinal application of dihydropyrano [3,2-b]pyrans and spiro-pyrano[3,2-b]pyrans by employing the reactivity of 5-hydroxy-2-(hydroxymethyl)-4hpyran-4-one. *Polycycl. Aromat. Compd.* **2022**, *42*, 5893–5937. [CrossRef]
6. Alam, S.; Sarkar, Z.; Islam, A. Synthesis and studies of antibacterial activity of pongaglabol. *J. Chem. Sci.* **2004**, *116*, 29–32. [CrossRef]
7. Aytemir, M.D.; Erol, D.D.; Hider, R.C.; Özalp, M. Synthesis and evaluation of antimicrobial activity of new 3-hydroxy-6-methyl-4-oxo-4H-pyran-2-carboxamide derivatives. *Turkish J. Chem.* **2003**, *27*, 757–764.
8. Mahdavi, S.M.; Habibi, A.; Dolati, H.; Mohammad, S.; Sardari, S.; Azerang, P. Synthesis and antimicrobial evaluation of 4H-pyrans and schiff bases fused 4H-pyran derivatives as inhibitors of mycobacterium bovis (BCG). *Iran. J. Pharm. Res.* **2018**, *17*, 1229–1239.
9. Randhawa, P.; Farasati, N.A.; Huang, Y. BK virus replication in vitro: Limited effect of drugs interfering with viral uptake and intracellular transport. *Antimicrob. Agents Chemother.* **2007**, *51*, 4492–4494. [CrossRef]
10. Akhlaghi, Z.; Naimi-Jamal, M.R.; Panahi, L.; Dekamin, M.G.; Far, B.F. Solvent-free mechanochemical multicomponent preparation of 4H-pyrans catalyzed by $Cu_2(NH_2\text{-BDC})_2(DABCO)$ metal-organic framework. *Heliyon* **2023**, *9*, e13522. [CrossRef]
11. Aytemir, M.D.; Çalış, Ü. Synthesis of some novel Mannich bases derived from allomaltol and evaluation of their anticonvulsant activities. *Hacettepe Univ. J. Fac. Pharm.* **2007**, *27*, 1–10.

12. Kaplan, J.; Verheijen, J.C.; Brooijmans, N.; Toral-Barza, L.; Hollander, I.; Yu, K.; Zask, A. Discovery of 3,6-dihydro-2H-pyran as a morpholine replacement in 6-aryl-1H-pyrazolo[3,4-d]pyrimidines and 2-arylthieno[3,2-d]pyrimidines: ATP-competitive inhibitors of the mammalian target of rapamycin (mTOR). *Bioorg. Med. Chem. Lett.* **2010**, *20*, 640–643. [CrossRef] [PubMed]
13. Bonsignorel, L.; Loyl, G.; Seccil, D.; Calignanoz, A. Synthesis and pharmacological activity of 2-oxo-(2H) 1-benzopyran-3-carboxamide derivatives. *Eur. J. Med. Chem.* **1993**, *28*, 517–520. [CrossRef]
14. Uenishi, J.; Ohmi, M. Total synthesis of (-)-laulimalide: Pd-catalyzed stereospecific ring construction of the substituted 3,6-dihydro[2H]pyran units. *Angew. Chem. Int. Ed.* **2005**, *44*, 2756–2760. [CrossRef] [PubMed]
15. Maulide, N. Six-membered rings with one heteroatom, and their fused carbocyclic derivatives. In *Comprehensive Heterocyclic Chemistry IV*, 1st ed.; Black, D., Cossy, J., Stevens, C., Eds.; Elsevier: Amsterdam, The Netherlands, 2021; Volume 7, pp. 491–511.
16. Mousavi, M.R.; Maghsoodlou, M.T.; Noori, F.; Hazeri, N. A facile and efficient synthesis of tetrahydrobenzo[b]pyrans using sucrose as green, inexpensive, natural and biodegradable catalyst. *Org. Chem. Res.* **2015**, *1*, 66–71.
17. Baker, C.D.L.; Fawcett, J.; Insley, C.D.; Messenger, D.S.; Newland, C.L.; Overend, H.L.; Patel, A.B.; Shah, M.; Vara, B.; Virdee, D.; et al. Triol protection with 6-benzoyl-3,4-dihydro-(2H)-pyran. *Chem. Commun.* **2005**, 1883–1885. [CrossRef]
18. Joule, J.A.; Mills, K. *Heterocyclic Chemistry*, 5th ed.; John Wiley & Sons, Ltd.: Chichester, UK, 2010; pp. 1–689.
19. Babinszki, B.; Jakab, E.; Terjék, V.; Sebestyén, Z.; Várhegyi, G.; May, Z.; Mahakhant, A.; Attanatho, L.; Suemanotham, A.; Thanmongkhon, Y.; et al. Thermal decomposition of biomass wastes derived from palm oil production. *J. Anal. Appl. Pyrolysis* **2021**, *155*, 105069. [CrossRef]
20. Chithiravel, R.; Rajaguru, K.; Muthusubramanian, S.; Bhuvanesh, N. Characterization of the major isomers of substituted tetrahydro-2H-pyrans from 1,3,5-triarylpentane-1,5-diols by p-toluenesulfonic acid treatment. *J. Mol. Struct.* **2018**, *1156*, 684–689. [CrossRef]
21. Cano, R.; Ramón, D.J.; Yus, M. Unmodified nano-powder magnetite or iron(III) oxide catalyze the easy and fast synthesis of 4-substituted-4H-pyrans. *Synlett* **2011**, *14*, 2017–2020. [CrossRef]
22. Uenishi, J.; Ohmi, M.; Ueda, A. Pd^{II}-catalyzed stereospecific formation of tetrahydro- and 3,6-dihydro [2H] pyran rings: 1,3-chirality transfer by intramolecular oxypalladation reaction. *Tetrahedron Asymmetry* **2005**, *16*, 1299–1303. [CrossRef]
23. Maddila, S.; Kerru, N.; Jonnalagadda, S.B. Recent progress in the multicomponent synthesis of pyran derivatives by sustainable catalysts under green conditions. *Molecules* **2022**, *27*, 6347. [CrossRef]
24. Ahmad, I.; Jasim, S.A.; Yasin, G.; Al-Qargholi, B.; Hammid, A.T. Synthesis and characterization of new 1,4-dihydropyran derivatives by novel Ta-MOF nanostructures as reusable nanocatalyst with antimicrobial activity. *Front. Chem.* **2022**, *10*, 967111. [CrossRef] [PubMed]
25. Wellington, A. Gas-phase Pyrolysis of 3,4-dihydro-2H-pyran. *J Chem. Soc. A* **1969**, 2584–2587. [CrossRef]
26. Caton, C.S. The thermal decomposition of 6-methyl-3,4-dihydro-2H-pyran. *J. Am. Chem. Soc.* **1969**, *91*, 7569–7572. [CrossRef]
27. Frey, H.M.; Hopkins, R.G.; Isaac, N.S. The thermal unimolecular decomposition of 2-methoxy-3,4-dihydro-2H-pyran. *J. Chem. Soc. Perkin Trans.2* **1972**, *73*, 2082–2084. [CrossRef]
28. Collins, J.F.; Frey, H.M.; Isaacs, N.S. The thermal decomposition of cis- and trans-2-methoxy-4-methyl-3,4-di hydro-2H-pyran. *J. Chem. Soc. Perkin Trans. 2* **1975**, *2*, 1–3. [CrossRef]
29. Bailey, I.M.; Frey, H.M. Thermal unimolecular decomposition of 2-ethoxy-3,4-dihydro-2H-pyran. *J. Chem. Soc. Perkin Trans. 2* **1977**, 870–872. [CrossRef]
30. Frey, H.M.; Lodge, S.P. Thermal decomposition of 3,6-dihydro-2H-pyran. *J. Chem. Soc. Perkin Trans. 2* **1979**, 1463–1464. [CrossRef]
31. Frey, H.M.; Pottinger, R.; Carless, H.A.J.; Lingley, D.J. The thermal decomposition of cis-2,6-dimethyl-3,6-dihydro-2H-pyran. *J. Chem. Soc. Perkin Trans. 2* **1979**, 1460–1462. [CrossRef]
32. Frey, H.M.; Watts, H.P. The thermal decomposition of 4-methyl-3,6-dihydro-2H-pyran. *Int. J. Chem. Kinet.* **1981**, *13*, 729–733. [CrossRef]
33. Taylor, R. The mechanism of thermal eliminations. Part 25. Arrhenius data for pyrolysis of isochroman-3-one, benzyl methyl ether, 2-hydroxyethylbenzene, phenyl acetate, and 3,4-dihydro-2H-pyran. *J. Chem. Soc. Perkin Trans.* **1988**, *2*, 183–189. [CrossRef]
34. Saito, K.; Adachi, K.; Watanabe, M.; Shimofuji, K.; Imamura, A. The thermal unimolecular decomposition of 3,4-dihydro-2H-pyran behind reflected shock waves. *Chem. Phys. Lett.* **1990**, *165*, 383–385. [CrossRef]
35. Alvarez-Aular, A.; Cartaya, L.; Maldonado, A.; Coll, D.S.; Chuchani, G. The kinetics and mechanism of the homogeneous, unimolecular gas-phase elimination of 2-(4-substituted-phenoxy)tetrahydro-2H-pyranes. *J. Phys. Org. Chem.* **2017**, *31*, e3778. [CrossRef]
36. Adamo, C.; Barone, V. Toward reliable density functional methods without adjustable parameters: The PBE0 model. *J. Chem. Phys.* **1999**, *110*, 6158–6170. [CrossRef]
37. Ditchfield, R.; Hehre, W.; Pople, J. Self-Consistent Molecular-Orbital Methods. IX. An Extended Gaussian-Type Basis for Molecular-Orbital Studies of Organic Molecules. *J. Chem. Phys.* **1971**, *54*, 724–728.
38. Frisch, M.J.; Trucks, G.W.; Schlegel, H.B.; Scuseria, G.E.; Robb, M.A.; Cheeseman, J.R.; Scalmani, G.; Barone, V.; Mennucci, B.; Petersson, G.A.; et al. *Gaussian 09, Revision B.01*; Gaussian, Inc.: Wallingford, CT, USA, 2010.
39. Fukui, K. A formulation of the reaction coordinate. *J. Phys. Chem.* **1970**, *74*, 4161–4163. [CrossRef]
40. Merrick, J.P.; Moran, D.; Radom, L. An evaluation of harmonic vibrational frequency scale factors. *J. Phys. Chem. A* **2007**, *111*, 11683–11700. [CrossRef]
41. McQuarrie, D.A.; Simon, J.D. *Molecular Thermodynamics*; University Science Books: Sausalito, CA, USA, 1999.

42. Glasstone, K.J.; Laidler, K.J.; Eyring, H. *The Theory of Rate Processes*, 1st ed.; McGraw-Hill: New York, NY, USA, 1941.
43. Benson, S.W. *The Foundations of Chemical Kinetics*; McGraw-Hill: New York, NY, USA, 1969.
44. Reed, A.E.; Weinhold, F. Natural bond orbital analysis of near-Hartree–Fock water dimer. *J. Chem. Phys.* **1983**, *78*, 4066–4073. [CrossRef]
45. Reed, A.E.; Curtiss, L.A.; Weinhold, F. Intermolecular interactions from a natural bond orbital, donor-acceptor viewpoint. *Chem. Rev.* **1988**, *88*, 899–926. [CrossRef]
46. Glendening, E.D.; Reed, A.E.; Carpenter, J.E.; Weinhold, F. *NBO*, version 3.1; University of Wisconsin: Madison, WI, USA, 1988.
47. Wiberg, K.B. Application of the pople-santry-segal CNDO method to the cyclopropylcarbinyl and cyclobutyl cation and to bicyclobutane. *Tetrahedron* **1968**, *24*, 1083–1096. [CrossRef]
48. Moyano, A.; Pericas, M.; Valentí, E. A Theoretical study on the mechanism of the thermal and the acid-catalyzed decarboxylation of 2-oxetanones (β-Lactones). *J. Org. Chem.* **1989**, *54*, 573–582. [CrossRef]